Proceedings of 9th IEEE International Conference
on CYBER Technology in Automation, Control, and Intelligent Systems
July 29- August 2, 2019, Suzhou, China

A Compact Asymmetrical Manipulator for Robotic Dentistry

Yufu Tao[#], Tianyi Zhang[#], Wenyutian Xu[#], Ho-Yin Tsang, Jing Li, *Student Member, IEEE,* and Zheng Wang*, *Senior Member IEEE*

***Abstract*— In contemporary society, there is an increasing gap between supply and demand for dental healthcare services. Meanwhile, robotics technology has the potential to greatly improving the working efficiency of dental surgeries hence filling the widening gap. However, newly-developed dental robots, which are based on existing large-sized industrial manipulators, have over-qualified workspace for dental applications. Thus, a miniaturized 6-Degree-of-Freedom robotic manipulator with tendon-driven mechanism was developed. With the manipulator being able of covering the whole human oral cavity, the overall size of the proposed manipulator has been successfully constrained in a 50x50x50cm^3 cube which is hardly possible for existing surgical manipulators. Meanwhile, the inverse kinematics algorithm was established through D-H modeling and was then implemented onto an operator console to achieve remote control. Moreover, a dental handpiece was utilized as the surgical end effector. The overall performance of the robotic system was validated with a fabricated prototype, where joints' linearity and torque transmission performances were analyzed from experimental results.**

I. Introduction

Nowadays, there is a rapid increase in the demand for dental healthcare services. According to a WHO report, nearly half of the world's population are affected by dental caries [1]. On the other hand, the labor shortage in professional dentists is severely growing and the long training cycle in the industry gives no promise to increase the number of dentists within a short period. For example, Hong Kong, home to 7 million people, is only served by 2280 registered dentist in 2017[2]. Moreover, conventional dental procedures like drilling and tooth milling are still conducted by dentists manually, some of the procedures are time-consuming and repetitive to perform. New technology is expected to solve the problems arisen from the dental healthcare industry.

With the increasing attention on dental healthcare services, several dental robotic systems have been developed. One of the most advanced products is Yomi, produced by Neocis and approved by FDA. Yomi can assist in dental implant surgery collaboratively [3]. Another dental robotic system produced by China could carry out implant surgery autonomously [4]. Powerful though they are, Yomi and the autonomous implant robot were developed from current industrial manipulators, whose workspace and payload capacities are far beyond needed for dental usage. Moreover, those industrial manipulators take up a considerable amount of space that are less economical to use in private clinics, notably in Hong Kong [5]. To meet with the potential needs for robotic systems in private clinics, as well as other circumstances where space constraints exist, or portability is required, a compact dental robotic system is proposed. The tendon-sheath mechanism is adopted to place the actuators outside the robot body, therefore, the size and weight of the robot could reduce significantly.

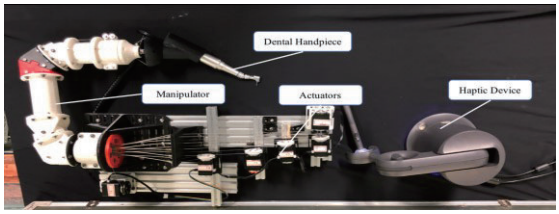

Fig. 1 Major functional units of the system

The proposed robotic manipulator for dental applications is featuring a compact size and a tailormade workspace, which could be teleoperated with a haptic device (Touch 3D Stylus). The system architecture and mechanical design are discussed in chapter 2. Chapter 3 covers the kinematics analysis and inverse kinematics algorithm of the finalized design. Tests on the performances of the manipulator are discussed in chapter 4.

II. System Design

The proposed dental robotic system shown in Fig. 1 consists of three functional units, namely a haptic device for teleoperation, a 6-Degree-Of-Freedom robotic manipulator and six motors (Feetech) to actuate the manipulator. The haptic device is programmed to obtain the dentist's hand motion and map the motion into the manipulator's workspace. Joint movement parameters would be calculated by the inverse kinematics analytically, and the corresponding actuation commands would be sent to the motors to drive the manipulator and perform surgical operations. In the mechanical design, the tendon-sheath mechanism and asymmetric configuration are introduced to miniaturize the manipulator and maximize the designed workspace to cover a real human oral cavity.

This work was partially supported by Hong Kong RGC-ECS Grant 27210315, ITF Grant ITS/140/18 and ITS/457/17FP, and HKU Seed Funding 201611160034.
All authors are with the Department of Mechanical Engineering, the University of Hong Kong, Hong Kong SAR, China.

Z. Wang is also with the Department of Mechanical and Energy Engineering, Southern University of Science and Technology, China. (Email: wangz@sustech.edu.cn).

*Corresponding author, e-mail: zwangski@hku.hk, Tel: +852-3917-7905, Fax: +852-2858-5415).

# These authors contributed equally to this work.

978-1-7281-0770-7/19/$31.00 © 2019 IEEE

A. System Architecture

The proposed robotic manipulator was prototyped with 3D printed components and tested with a control scheme. The overall system development process could be divided into two sections, including software system and hardware system, as shown in Fig. 2.

In the software system, manipulator motion is generated by master-slave control. Firstly, the dentist serves as the robot operator and his/her hand motion would be digitized by a haptic device and converted as the system input signal. Secondly, in the application program designed for the haptic device, digitized dentist hand motions were transferred into a 6-DOF spatial data and were mapped from the operator's workspace into the manipulator's workspace. Thirdly, the data would be processed by the manipulator control board, the Arduino Mega 2560, to generate corresponding motor commands. Lastly, the generated motor commands would be sent to the digital servo motors to drive the manipulator and output surgical operation motions. This way, the robot-assisted dental surgery could be achieved through a master-slave control configuration that allows the dentist to teleoperate dental robotic manipulator to perform surgical operations. During the inverse kinematics procedure, the control program was guided by the characteristics of the manipulator, which were concluded from kinematics analysis and relevant experiments, to connect the hardware and software in the system.

B. Tendon-sheath Mechanism

The proposed 6-DOF manipulator is composed of two cylindrical joints, two revolute joints, a wrist joint with 2 orthogonal DOF, and a dental handpiece acting as the end effector. From the base to the end effector, the joints were labelled as joint 1 to joint 6.

For miniaturization purpose, the tendon-sheath mechanism was adopted. Fig. 3 shows the arrangements of the tendons, which the red lines refer to the tendons and the bold yellow lines in Fig. 3(b) refer to tendon sheaths. In such mechanism as shown in Fig. 3, each joint is actuated by a pair of steel threads, also known as the tendons. The sheaths are auxiliary structures for enveloping the tendons to reduce the friction between tendons and the outer shells. The tendon actuation mechanism allowed the motors to be located outside the manipulator. Thus, powerful motors can be utilized without affecting the size of the manipulator.

C. Asymmetric Configuration

The modular design approach was adopted in the robotic system. Two revolute joints, joint 2 and joint 3, have similar structures, with identical mounting faces. Thus, as shown in Fig. 4, modularized spacers can be inserted to change the orientations of the joints and lengths of adjacent links conveniently.

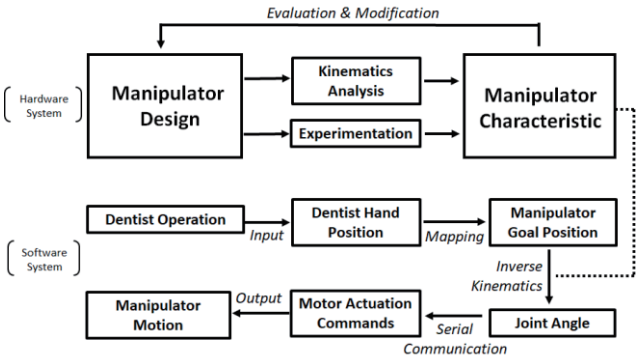

Fig. 2 System Architecture

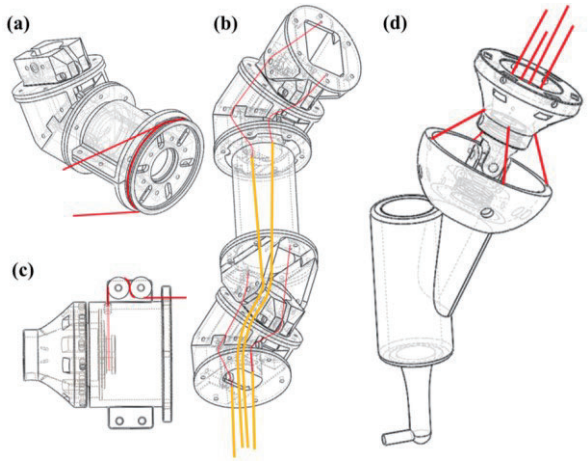

Fig.3 Tendon-sheath design of the proposed manipulator: (a). joint 1; (b). joint 2 & 3; (c). joint 2; (d). wrist-joint (joint 5 & 6).

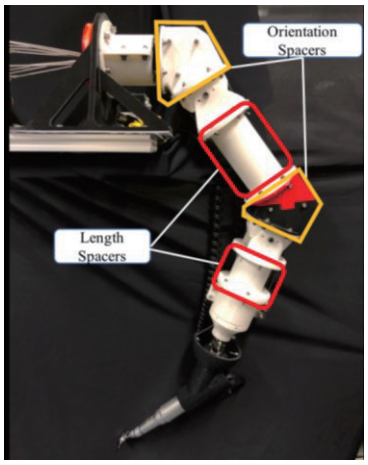

Fig. 4 Use of spacers on the proposed manipulator

Previous research [5-6] has proposed symmetric configurations, but the workspace could be limited by structural constraints. Inspired by human elbows, which only allow the forearm to move on one side of the upper arm, an asymmetrical configuration was adopted to achieve higher dexterity compared with the symmetrical structure. The asymmetric configuration was achieved by inserting two orientation spacers, as highlighted in red in Fig. 5, next to joint 2 & 3, to shift their range of rotation to one direction. A side view of the workspace in (b) shows that the thickness of the dome-shaped shell workspace can fully cover the human oral cavity.

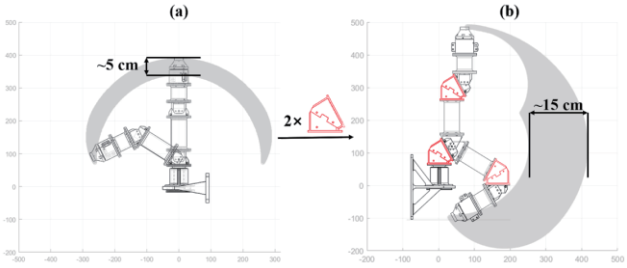

Fig. 5 Simulated workspaces: symmetric configuration (a) and asymmetric configuration (b) reshaped by two orientation spacers highlighted in red.

Table 1 List of symbols

L_i	Link length of the (i-1)-th joint and i-th link
α_i	The angle from Z_i to Z_{i+1} measured about X_i
a_i	The distance from Z_i to Z_{i+1} measured along X_i
d_i	The distance from X_{i-1} to X_i measured along Z_i
θ_i	The angle from X_{i-1} to X_i measured about Z_i
x_i	x coordinate of frame {i}
y_i	y coordinate of frame {i}
z_i	z coordinate of frame {i}
${}^i_jR$	Rotation matrix from frame {j} to frame {i}
${}^i_jT$	Transformation matrix from frame {j} to frame {i}
V	A vector V
V(i)	The i-th element of vector V
$\boldsymbol{P}^i_M$	A position vector P of point M relative to frame {i}
$\boldsymbol{V}^i_{N,M}$	A vector V from point N to point M relative to frame {i}
$\widehat{\boldsymbol{u}^i_{ee}}$	The unit vector representing the orientation of ee (end effector) relative to frame {i}

III. Kinematics Analysis

As mentioned above, the symmetric configuration proposed by previous research [5-6] results in physical limitations in the manipulator's workspace. An asymmetrical configuration was therefore adopted in the proposed manipulator. In this chapter, the schematic diagrams of both models (symmetric and asymmetric) are included in the respective sections, with coordinate frames and D-H parameters indicated in the diagrams. Only the inverse kinematics algorithm of the finalized asymmetric model was developed. Shown in the table below are symbols used in this chapter.

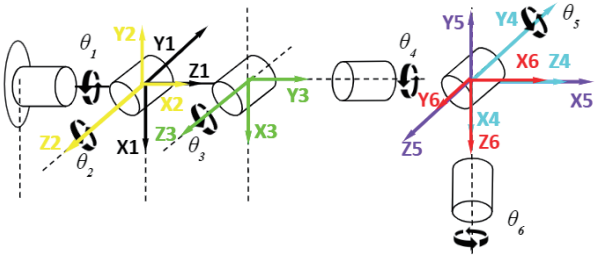

Fig. 6 Schematic diagram of the symmetric model

Table 2 D-H table of the symmetric model

Link i	α_{i-1}	a_{i-1}	d_i	θ_i	Joint angle q
1	0	0	82	q_1	$q_1 \in (0, 2\pi)$
2	π/2	0	0	$\pi/2 + q_2$	$q_2 \in (-2*\pi/3, 0)$
3	0	143.2	0	$-\pi/2 + q_3$	$q_3 \in (-\pi/3, \pi/3)$
4	-π/2	0	160	q_4	$q_4 \in (0, 2\pi)$
5	π/2	0	0	$\pi/2 + q_5$	$q_5 \in (-\pi/4, \pi/4)$
6	π/2	0	0	q_6	$q_6 \in (-\pi/4, \pi/4)$

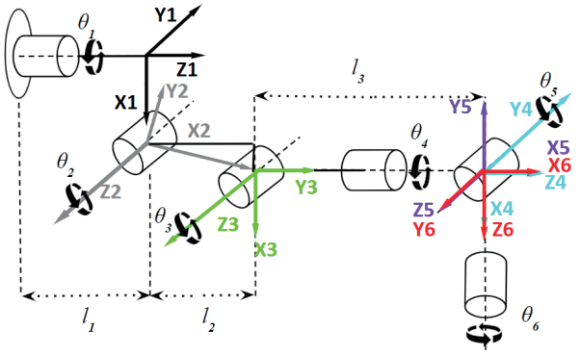

Fig. 7 Schematic diagram of the asymmetric model

Table 3 D-H table of the asymmetric model

Link i	α_{i-1}	a_{i-1}	d_i	θ_i	Joint angle q
1	0	0	40	q_1	$q_{1\in}(0, 2\pi)$
2	π/2	120	0	$13*\pi/30 + q_2$	$q_{2\in}(-23*\pi/33, 0)$
3	0	194	0	$-23*\pi/30 + q_3$	$q_{3\in}(-\pi/3, \pi/3)$
4	-π/2	0	176	q_4	$q_{4\in}(0, 2\pi)$
5	π/2	0	0	$\pi/2 + q_5$	$q_{5\in}(-\pi/4, \pi/4)$
6	π/2	0	0	q_6	$q_{6\in}(-\pi/4, \pi/4)$

Inverse kinematics algorithms based on the finalized asymmetric model are as follows.

$$\boldsymbol{P}^0_{ee} = {}^0_6R \cdot \widehat{\boldsymbol{P}^6_{ee}} \cdot |\boldsymbol{P}^6_{ee}| + \boldsymbol{P}^0_{6\,Org} \qquad (1)$$

In the robotic manipulator, origins of references {4}, {5} and {6} overlap.

$$\boldsymbol{P}_{ee}^{0} = {}_{6}^{0}R \cdot \widehat{\boldsymbol{P}_{ee}^{6}} \cdot |\boldsymbol{P}_{ee}^{6}| + \boldsymbol{P}_{4\,Org}^{0} \tag{2}$$

Numerical ${}_{6}^{0}R$ can be obtained from $\widehat{\boldsymbol{u}_{ee}^{0}}$ and $\widehat{\boldsymbol{u}_{ee}^{0}}$ by the formulas from (3) to (7)

$$\mathbf{v} = \widehat{\boldsymbol{u}_{ee}^{6}} \times \widehat{\boldsymbol{u}_{ee}^{0}} \tag{3}$$

$$\mathrm{c} = \widehat{\boldsymbol{u}_{ee}^{6}} \cdot \widehat{\boldsymbol{u}_{ee}^{0}} \tag{4}$$

$$\mathrm{vx} = \begin{bmatrix} 0 & -v(3) & V(2) \\ v(3) & 0 & -v(1) \\ -v(2) & -v(1) & 0 \end{bmatrix} \tag{5}$$

$$\mathrm{I} = \begin{bmatrix} 1 & 0 & 0 \\ 0 & 1 & 0 \\ 0 & 0 & 1 \end{bmatrix} \tag{6}$$

$${}_{6}^{0}R = I + vx + vx \cdot vx/(1+c) \tag{7}$$

$\boldsymbol{P}_{ee}^{0}$ and $\widehat{\boldsymbol{u}_{ee}^{0}}$ are numerical inputs from user interface. θ_1, θ_2 and θ_3 can be obtained by solving $\boldsymbol{P}_{ee}^{0} = {}_{6}^{0}R \cdot \widehat{\boldsymbol{u}_{ee}^{6}} \cdot |\boldsymbol{P}_{ee}^{6}| + \boldsymbol{P}_{4\,Org}^{0}$. θ_4, θ_5 and θ_6 can be obtained by solving ${}_{6}^{0}R = {}_{3}^{0}R \cdot {}_{6}^{3}R$, where ${}_{3}^{0}R$ is written in numerical form with solved θ_1, θ_2 and θ_3.

IV. Experimentation

In this section, the experimental setup and results are discussed, which include two experiments, one on the motion transmission and the other on torque transmission. Results from motion transmission are the ratios between each actuator's motion and the corresponding joint's motion, which guide the control program to give an estimation of the actual position for the manipulator's tip point. Results from torque transmission are utilized for payload analysis.

A. Motion Transmission

The motion transmission refers to the transmission relation between joints and the motors. The first four joints were chosen as the testing objects, which were tested individually. During the test, the unrelated joints were fixed at their default position, only the joint to be tested was moveable and was connected to a rotary encoder to record the movement of joints. An Arduino board was used to control the motion of motors and record the movement of the motor based on the built-in sensors. The setup of the experimentation of motion transmission is shown in Fig. 8.

The motion transmission results are shown in Fig. 9, we can see joint motion matches the movement of motors with a linear relation. The slopes of the four lines are different because of the different standards of mounting for each joint. The standard is that the further the joint is from the end-effector, the larger the torque is applied to the joint, therefore, the size of mounting of distant joints were made larger to reduce the torque applied to the motor.

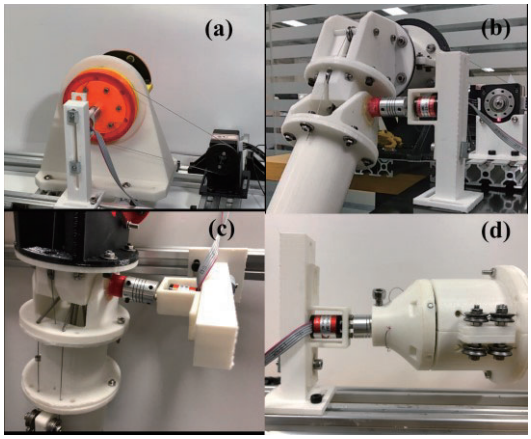

Fig. 8 Experimental setup of the motion transmission test. (a) Setup of the first joint (b) Setup of the second joint (c) Setup of the third join (d) Setup of the fourth joint

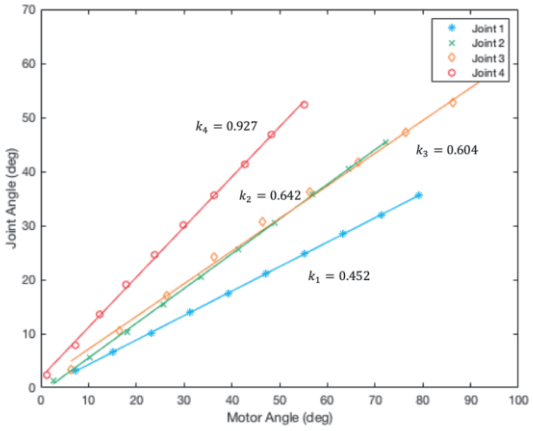

Fig. 9 Results of motion transmission experiment, k_i represents the i-th joint

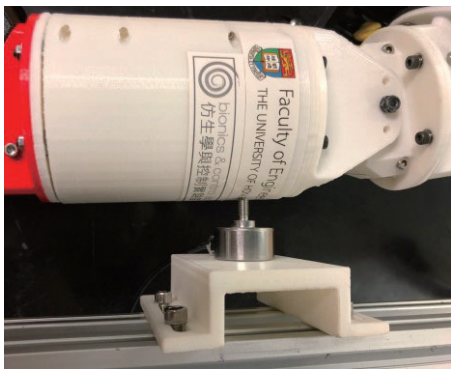

Fig. 10 Experimental setup of the torque transmission test using the first revolute joint as an example

B. Torque Transmission

The torque transmission refers to the relation between the input torque and the output torque of the joint. During the test, a force sensor was used to measure the output force of the joint at a known point and the torque is calculated by multiplying the output force with the perpendicular distance between the point and the rotational axis. As the input torque was gradually increased, the output torque of the joint was measured. The experimentation setup of the first revolute joint is shown in Fig. 10.

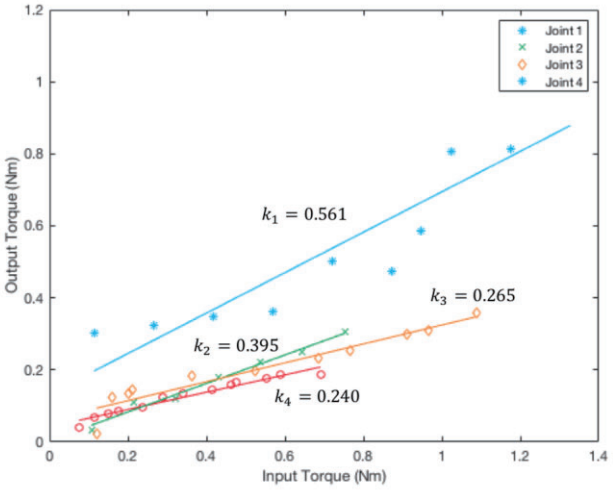

Fig. 11 Results of torque transmission experiment, k_i represents the i-th joint

The experimental results are shown in Fig. 11. The relationship between input and output torque can approximately follow a linear relationship within the measurement range. In this test, the maximum output torque of the fourth joint is 0.18 Nm. Considering the extension that holds the end-effector, the payload of the manipulator is 0.6 kg. The result showed that the output torques of joints have fulfilled the requirements of holding a dental handpiece properly.

V. Conclusion

In recent years, development in robotics has presented a solution for bridging the gap between the demand for high quality dental healthcare service and supply for qualified dentists. However, existing dental robotic systems, as well as those currently under development or research, are usually based on commercially available industrial robot platforms, whose size and energy consumption are unfit in circumstances where space and acceptable running overhead are limited, for instance, the private clinics in the city of Hong Kong. Thus, compact robotic system design for dental uses is proposed in this paper.

In the design of the manipulator, the tendon-driven actuation method was adopted, allowing more powerful motors to be utilized without affecting the size of the manipulator. An asymmetric configuration has optimized the manipulator's workspace, to make sure a human oral cavity could be covered. Multiple tests were carried out on the prototypes to examine its performance and weaknesses. The linearity test showed that the transmission from the motors to the joints was ideal enough to be treated as linear. However, the hysteresis test showed that hysteretic property was disadvantageous to the repeatability of the system, but the pretension test showed that the effect could be scaled down by applying proper pretension.

The finalized model of the manipulator is about the same size as a human upper limb. In storage term, the manipulator, as well as other auxiliary components, can be fitted into a container about the size of a 25-inches suitcase. Thus, the manipulator can be easily stored in private clinics and may even be portable.

As mentioned above, significant hysteresis and loss of torque were observed in torque transmission tests. These problems were induced by the tendon-driven mechanism. Also, for mathematical convenience in the development and testing of inverse kinematics algorithm, the relationship between joint angle and the motor angle was approximately considered linear.

Acknowledgment

This project is under supervision from Dr. Wang, Zheng. His support is crucial to the completion of this project. He actively held meetings with our group members monthly which were fruitful and constructive. Whenever a gooseneck was met somewhere in between, his advice was always enough in clearing the misconceptions and confusions that rose from the topic. Dr. Wang has provided us new perspectives in the development of the prototype for our mechanical designs, as well as warnings about the obstacles that we may run into during the design processes. We are deeply grateful for his guidance. Without his support and insight, our achievements on this project would have never been possible.

We would like to express our sincere gratitude to Ms. Li, Jing, who was actively involved in our project as a senior coordinator. Her role was indeed irreplaceable in this project. We would also like to thank all the senior students in the lab for assistance and support they've given.

References

[1] Kassebaum, N. J., Bernabé, E., Dahiya, M., Bhandari, B., Murray, C. J. L., & Marcenes, W. "Global Burden of Untreated Caries: A Systematic Review and Metaregression," *Journal of Dental Research*, vol. 94, no. 5, pp. 650-658, 2015. https://doi.org/10.1177/0022034515573272

[2] Gao, S. S., Chen, K. J., Duangthip, D., Lo, E., & Chu, C. H. (2018). Oral Health Care in Hong Kong. Healthcare (Basel, Switzerland), 6(2), 45. doi:10.3390/healthcare6020045

[3] Sreelekshmi, S., Varghese, K., Abraham, J.P. and Jaysa, J.J., 2017. *Applications Of Robotics In Prosthodontics–A Review.*

[4] Alice, Yan. "Chinese robot dentist is first to fit implants in patient's mouth without any human involvement." *South China Morning Post.* Sept, 21, 2017. [Online] Available:

http://www.scmp.com/news/china/article/2112197/chinese-robot-dentist-first-fit-implants-patients-mouth-without-any-human

[5] J. Li, W. Y. H. Lam, R. T. C. Hsung, E. H. N. Pow, and Z. Wang, "A Customizable, Compact Robotic Manipulator for Assisting Multiple Dental Procedures," *2018 3rd International Conference on Advanced Robotics and Mechatronics (ICARM)*, 2018.

[6] J. Li, Z. Shen, W. Xu, W. Y. H. Lam, R. T. C. Hsung, E. H. N. Pow, K. Kosuge, Z. Wang "A Compact Dental Robotic System Using Soft Bracing Technique" in *IEEE Robotics and Automation Letters*, Volume. 4, Issue 2, 23 Jan 2019, pp. 1271-1278